

Viewing the Interior of a Single Molecule: Vibronically Resolved Photon Imaging at Submolecular Resolution

Chi Chen, Ping Chu, C. A. Bobisch, D. L. Mills, and W. Ho*

Department of Physics and Astronomy and Department of Chemistry, University of California, Irvine, California 92697, USA
(Received 26 June 2010; revised manuscript received 24 September 2010; published 15 November 2010)

We report the spatial imaging of the photon transition probability of a single molecule at submolecular resolution. Photon imaging of a ringlike pattern is further resolved as two orthogonal vibronic transitions after incorporating spectral selectivity. A theoretical model and the calculated intensity images reveal that the transition probability is dominated by the symmetry of the positions of the tip and the transition dipole moment. This imaging technique enables the probing of the electronic and optical properties in the interior of a single molecule.

DOI: 10.1103/PhysRevLett.105.217402

PACS numbers: 78.68.+m, 07.79.Cz, 68.37.Ef, 78.60.Fi

Probing single molecules by optical spectroscopy and microscopy has become an important approach in the study of biophysics, polymers, and nanomaterials [1]. This approach removes ensemble averaging and reveals characteristics of a selected molecule, including its interactions with the local environment. However, the spatial resolution of fluorescence microscopy is restricted by the diffraction limit even though optical detection reached the single molecule level two decades ago [2]. With the development of near field optical techniques [3] and superresolution optical imaging [4], the resolution has improved to a few tens of nanometers but is still above the size of a small molecule. Until now, no experimental strategy has resolved the internal structure of an emitting fluorophore.

Light emission induced by tunneling electrons has reached sub-Ångstrom precision with a scanning tunneling microscope (STM) [5,6]. Since the excitation, relaxation, and emission processes are all entangled, the photon intensity at each pixel is interpreted as the transition probability at each injection location. The spatial resolution of this “STM photon microscopy” is unmatched by any other optical techniques.

For single molecules on metal surfaces, the intrinsic emission would be quenched by strong electronic interactions with the substrate. By introducing a thin insulating layer [7–9] or by decoupling via a molecular multilayer [10], intramolecular transitions with vibronic features have been successfully detected from porphyrin molecules and C_{60} islands. However, the spatially resolved photon imaging of the vibronic emission has not been achieved.

Here, we report real space, spectrally resolved photon microscopy of intramolecular optical transitions with submolecular resolution on a single magnesium porphine (MgP) molecule adsorbed on an ultrathin Al_2O_3 grown on the NiAl(110) surface. The spatial distribution of the photon transition probability directly corresponds to the orbitals of the MgP molecule. Our view is that our experiment has reached the ultimate resolution and also it reveals

new fundamental aspects of molecular radiative transitions as substantiated by a theoretical calculation.

The experiments were conducted with a homebuilt STM operated at 10 K in ultrahigh vacuum. Tip and sample preparation follow previous reports [6,7]. A silver tip was prepared by electrochemical etching and the MgP molecules were purchased from Frontier Scientific, Inc. In the experiment, MgP molecules were thermally evaporated onto the cold partially oxidized NiAl(110) surface at 10 K. The emitted photons were collected with a lens mounted inside the UHV chamber and then guided to the detection system. The detector could be switched between an avalanche photodiode (APD, Perkin Elmer SPCM-AQR) and a spectrometer (Princeton Instruments, Acton SP2300A) equipped with a liquid nitrogen cooled CCD (Princeton Instruments, Spec-10:100B). All photon images and optical spectroscopy were done under constant current condition.

STM topographies with corresponding photon (intensity) images taken simultaneously are shown in Fig. 1. In the large oxide area [Fig. 1(a)], only four of 11 molecules can emit photons under the scanning condition (2.2 V, 0.2 nA). Besides MgP molecules, some other small adsorbates or defects are emissive as well when excited by the tunneling electrons (e.g., three bright spots at the lower middle). By zooming into the selected area in Fig. 1(b), emitting and nonemitting molecules could be clearly distinguished. The MgP molecule with the shape of two lobes is not emissive while the other symmetric MgP emit photons.

The photon image of a single MgP molecule appears as a ringlike pattern with four bright maxima and a relatively dark center [Fig. 1(c)]. This ringlike pattern is common for every molecule showing vibronic peaks in the emission spectrum [11]. Comparison of the photon image with MgP molecular structure [Fig. 2(d)] reveals that the optical transition occurs at the porphyrin macrocycle and the central Mg ion plays only a minor role. These images provide a visualization of the basic concepts of chromophores and

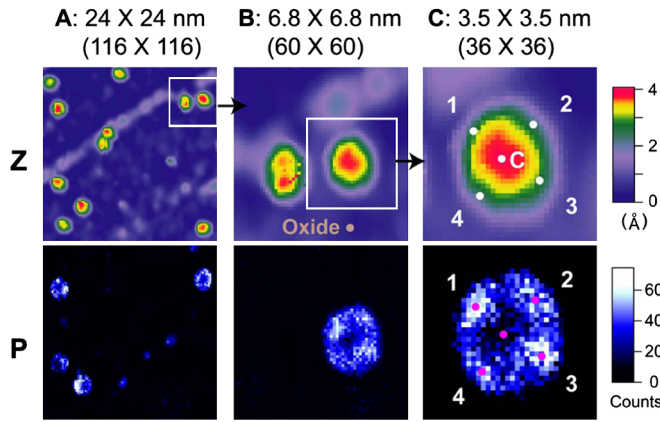


FIG. 1 (color online). Topographic images (top, Z) and photon images (bottom, P) taken simultaneously. Image sizes and resolutions are labeled at the top of each figure. Same color pallets are used from (A) to (C) but the indicated absolute values of both Z and P are only for (C). All images are acquired under 2.2 V and 0.2 nA. Integration time of the APD at each pixel is 0.1 s in (A) and 0.2 s in (B) and (C). The dots and numbers in (C) indicate the positions where the spectra in Fig. 2 were taken.

fluorophores that have been discussed in chemistry textbooks for many years.

In contrast to the four maxima in the photon images, the topography of MgP shows only twofold symmetry with elongation along one diagonal. To understand this difference and the origin of the four bright maxima, additional emission spectra [Fig. 2(a)] provide crucial physical insight. We have examined emission spectra taken at the points indicated in Fig. 1(c). At the center of MgP, the spectrum is relatively weak and featureless, which is consistent with the “doughnut hole” observed in the photon image. On the other hand, the spectra taken at the four maxima all contain sharp features. The four spectra can be separated into two groups: type-I emission which has one strong main peak (position P1 and P3) and type-II (position P2 and P4) which show equally spaced multi-peaks.

In the type-II spectra, these equally spaced peaks in energy are assigned to vibronic transitions originating from coupling of vibrational modes to the electronic transition [7,8]. Fitting the sequence peak positions yields a slope of 47 ± 2 meV (379 ± 16 cm^{-1}), which is assigned to the pyrrole rotation or tilt modes [12]. On the other hand, in positions P1 and P3, type-I spectra is dominated by one strong peak. It is not possible to perform a clear vibrational analysis since only a second peak with spacing ~ 89 meV (718 cm^{-1}) could be identified. However, the spacing is larger than that of type-II progression. This suggests weaker binding to the substrate, which would lead to higher vibrational frequencies, or another mode.

For all the MgP showing vibronic transitions, it is found that type-I emission always occurs along the molecular long axis of the topography, while type-II occurs along the short axis. This asymmetry in both vibronic coupling

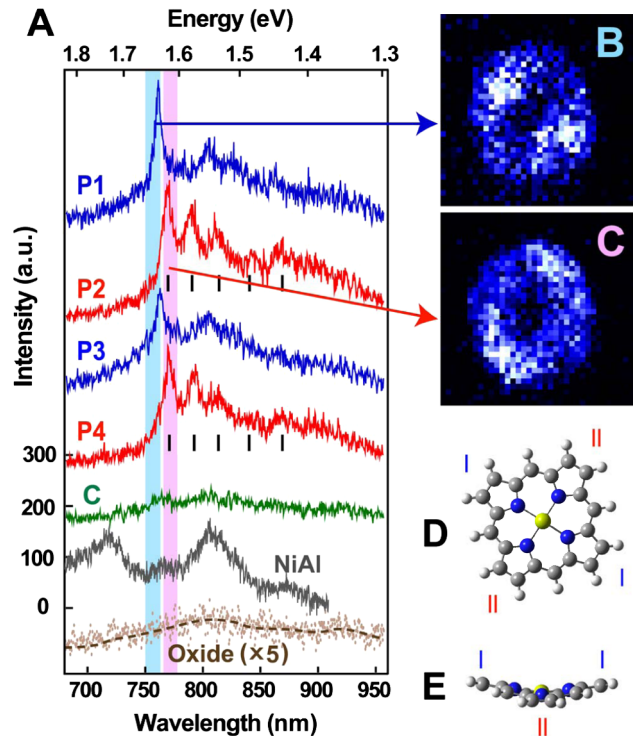


FIG. 2 (color online). (A) Vibronically resolved emission spectra taken at five positions inside the MgP molecule [P1-P4 and center; positions are indicated in Fig. 1(c)], oxide background ($\times 5$), and metal background (NiAl). Colors are used to distinguish type-I (blue) and type-II (red) spectra in the online edition. All spectra are taken under 2.3 V bias and 0.25 nA tunneling current with 300 s accumulation time. (B),(C) Photon images of individual vibronic peaks taken under 2.3 V bias and 0.4 nA tunneling current. The size for all the images is $35 \text{ \AA} \times 35 \text{ \AA}$. Photon image of type-I peak from 750 to 763 nm (B) shows orthogonal symmetry compare to that of type-II transition from 766 to 778 nm (C). CCD integration time at each pixel is 1.0 s. (D),(E) Top and side view of the molecular structure of MgP. Its orientation is aligned to the photon images in (B) and (C). I and II label the positions of type-I and type-II emission, respectively.

and the elongated topography could be attributed to the structural deformation of the molecule, which reduces MgP symmetry from planar D_{4h} to nonplanar twofold symmetry. Among all the recognized porphyrin conformations [13], the saddle form is the most likely conformation that is consistent with the experimental findings. The structure of the saddle shape MgP is shown in Fig. 2(e), and the positions of type-I and type-II sequences are labeled as well.

Different vibronic coupling caused by structural deformation within a molecule is revealed spatially through spectrally resolved imaging. When only a type-I peak wavelength is selected, the photon image shows twofold symmetry with a nodal plane across the center of the molecule [Fig. 2(b)]. When the selected wavelength is at the peak of type-II spectrum, the emission maxima are

located at the other diagonal of the MgP [Fig. 2(c)]. The spatial distributions of type-I and type-II transitions are nearly orthogonal to each other. Furthermore, the threshold wavelengths of the two spectra are separated by only a few nanometers. We propose that there are two nearly degenerate, orthogonal orbitals that are involved in the optical transitions.

Besides optical emission, STM provides electronic state information through dI/dV spectra. In Fig. 3(a), features in the dI/dV spectra are quite similar everywhere inside the MgP except for small shifts of the orbital onsets. For positive bias, the state higher than ~ 1.8 V could be attributed to the oxide background at the first glance. However, from the photon excitation curves shown in Fig. 3(b), it is found that the vibronic emission of the MgP starts at ~ 1.8 V and reaches its highest intensity around 2.2–2.3 V. Based on this observation, the onset of the lowest unoccupied molecular orbital (LUMO) is identified at ~ 1.8 V.

Aside from the LUMO state, a series of vibronic peaks around 0.4–0.8 V is associated with the highest occupied molecular orbital (HOMO), which is originally located below the Fermi level in the negatively biased sample (from ~ -0.1 V) [14]. As the applied bias increases, the electrostatic potential across the oxide (E_{ox}) becomes large

enough to lift the HOMO state above the Fermi level [Fig. 3(c)]. This results in a set of sharp vibronic peaks due to a dramatic change in the overall conductance.

As a consequence, the HOMO becomes the empty “hole state.” When the bias is increased high enough (> 1.8 V) to resonantly inject an electron into the LUMO, the intramolecular emission occurs between Fig. 3(d). This picture is not in conflict with the LUMO + 1 to LUMO mechanism proposed by Qiu *et al.* [7] due to the different alignment of the molecular orbitals relative to the Fermi level for the various molecular conformations on the inhomogeneous oxide layer.

From our molecular orbital calculations as well as from the literature [15,16], the LUMO of MgP is not a single orbital but consists of two degenerate, orthogonal orbitals. On the inhomogeneous oxide surface, a broken degeneracy causes a small spectral shift of these two LUMO states, which is too small to be resolved in the dI/dV spectrum or topography [17]. However, the different vibronic couplings between each of these two LUMO states with the HOMO state give rise to distinct differences in the photon spatial images.

Here we develop a generalized model to simulate these observations based on previous work [18,19]. Starting from the molecule in free space, the radiative lifetime of excited state ψ_I is controlled by the electric dipole matrix element $P_{\alpha}^{\text{IF}} = e \int d^3r \psi_F(\vec{r}) * r_{\alpha} \psi_I(\vec{r}) = \int d^3r P_{\alpha}^{\text{IF}}(\vec{r})$. If the molecule is under the tip and above the substrate, a distant observer will see a total radiating dipole moment $\vec{P}^{\text{IF}}(\text{tot})$ that consists of the molecular transition dipole, supplemented by the dipole moment associated with the (dynamic) image charges induced in the tip and substrate combination (Fig. 4). If a point dipole $d^3P_{\alpha}^{\text{IF}}(\vec{r})$ is placed at \vec{r} , then the total dipole moment is written $\sum_{\beta} S_{\alpha\beta}(\vec{r}) d^3P_{\beta}^{\text{IF}}(\vec{r})$ where classical phenomenology is used to describe the image charges. We calculate the radiative lifetime of the excited state through the Fermi golden rule using $P_{\alpha}^{\text{IF}}(\text{tot}) = \int \sum_{\beta} S_{\alpha\beta}(\vec{r}) d^3P_{\beta}^{\text{IF}}(\vec{r})$. To generate $S_{\alpha\beta}(\vec{r})$, we describe the local environment near the bottom of the tip by approximating the tip by a large sphere with radius of curvature R and dielectric constant $\epsilon_T(\omega)$ with substrate taken as a plane with dielectric constant $\epsilon_S(\omega)$. Expressions for $S_{\alpha\beta}(\vec{r})$ may be generated through use of bispherical coordinates. Details are found elsewhere [20]. We use orbitals of the molecule in free space, generated by Gaussian 03 (G03) as before [21]. In the results below, the radius of curvature of the tip has been taken to be 2 nm [22]. Other parameters like tip and substrate materials and molecule to substrate distance are the same as experimental conditions. Test calculations show an oxide layer has little influence on the image charges. The intensity contrast as calculated in Fig. 4 is decreased as the radius of curvature is increased. In the experiment, blunter tips also lead to a loss in contrast. In addition, asymmetric photon images and topography are obtained for irregular tips.

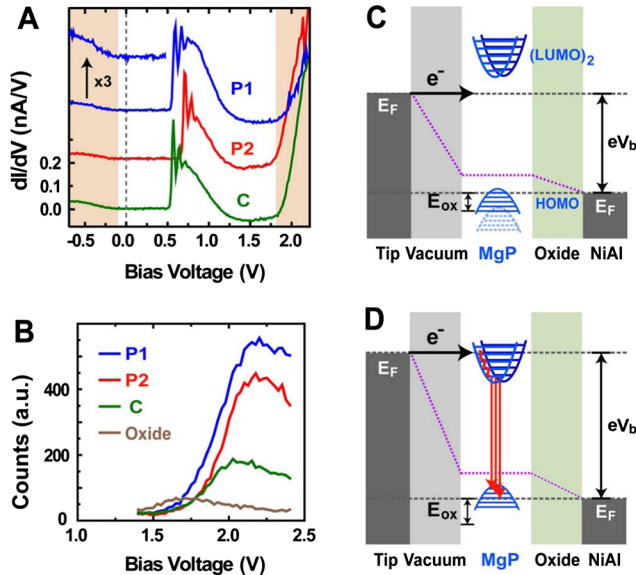


FIG. 3 (color online). dI/dV spectra, excitation spectra, and the illustrations of the LUMO-HOMO transitions mechanism. (A) dI/dV spectra at P1, P2, and center of the MgP as indicated in Fig. 1(c). All the color codings are the same as Fig. 2. (B) Photon excitation spectra as a function of bias voltage. Notice that the oxide background emission reaches its maximum at 1.7 V. This slightly affects the determination of the LUMO onset. (C)–(D) Schematic illustrations of LUMO-HOMO transition. (C) At this bias voltage, the HOMO is being lifted above the Fermi level by the electrostatic potential and becomes an empty state. (D) The vibronic transition occurs when the bias is high enough to inject electrons into LUMO (> 1.8 V).

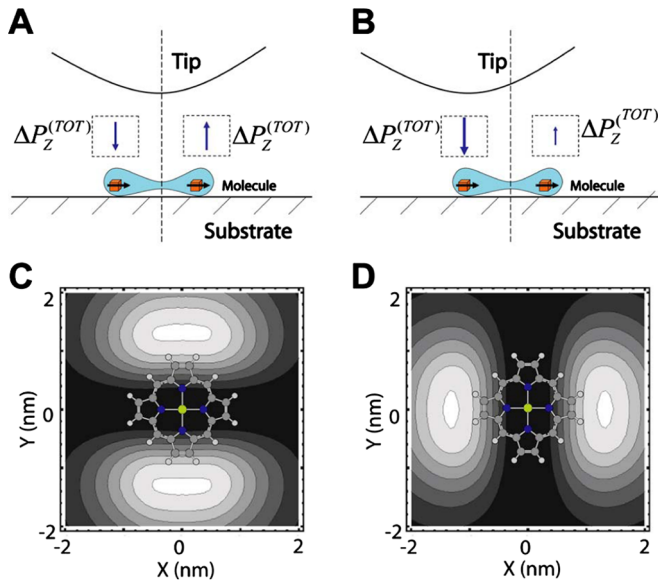


FIG. 4 (color online). (A),(B) Mechanism for generating a net perpendicular dipole moment, when the transition dipole is parallel to the surface. If the tip is centered over the molecule, the contribution from the two point dipole illustrated in (A) cancel, whereas they do not when the tip is off center, as shown in (B). (C),(D) The simulated intensity images of light emission from the two orthogonal LUMO states. The intensity is maximized when tip is off from the center of the molecule.

For the LUMO to HOMO transition, and also for the LUMO + 1 to LUMO, the transition dipole is parallel to the plane of the molecule and hence to the substrate surface. Such a dipole is screened strongly by the dynamic image charges [18,19]. We find the dominant contribution to the total dipole moment comes from its perpendicular component. When the tip is off center, symmetry allows a net total dipole moment, as shown in Fig. 4, whereas the total perpendicular dipole moment vanishes when the tip is placed over the center of the molecule. Qualitatively, the calculation matches well with our experimental results and gives a physical picture about how the symmetry relation between tip and molecular orbital determines the total transition probability.

Based on the STM photon microscopy technique, photon imaging of a single molecule has achieved submolecular resolution. Two types of highly localized vibronic coupling reveal the existence of two orthogonal but nearly degenerate LUMO states. We believe that our experiment advances single molecule spectroscopy and microscopy. This approach provides the possibility of visualizing intrinsic emission properties of a single molecule and the effects of its local environment as well. Our STM-based experiments not only remove ensemble averaging, the spatial inhomogeneity of optical transitions inside a single

molecule is revealed. Furthermore, with the STM's ability to manipulate molecules, our method leads to unprecedented opportunities to investigate the fundamental mechanisms of intermolecular fluorescence resonant energy transfer (FRET) and other important electron-molecule-photon coupled system.

This work is supported by the Chemical Science, Geo- and Bioscience Division, Office of Science, U.S. Department of Energy, under Grant No. DE-FG02-04ER1595, and the NSF Center for Chemical Innovation on Chemistry at the Space-Time Limit (CaSTL) under Grant No. CHE-0802913. Additional support is provided to C. A. B. by the Alexander von Humboldt Foundation. We have benefited from insightful discussions with R. Wu.

*Corresponding author.

wilsonho@uci.edu

- [1] R. Rigler and H. Vogel, *Single Molecules and Nanotechnology* (Springer-Verlag, Berlin, 2008).
- [2] W.E. Moerner and L. Kador, *Phys. Rev. Lett.* **62**, 2535 (1989).
- [3] L. Novotny and B. Hecht, *Principles of Nano-optics* (Cambridge University Press, Cambridge, 2006).
- [4] S. W. Hell, *Science* **316**, 1153 (2007).
- [5] R. Berndt *et al.*, *Science* **262**, 1425 (1993).
- [6] C. Chen, C. A. Bobisch, and W. Ho, *Science* **325**, 981 (2009).
- [7] X.H. Qiu, G. V. Nazin, and W. Ho, *Science* **299**, 542 (2003).
- [8] S. W. Wu, G. V. Nazin, and W. Ho, *Phys. Rev. B* **77**, 205430 (2008).
- [9] E. Cavar *et al.*, *Phys. Rev. Lett.* **95**, 196102 (2005).
- [10] Z. C. Dong *et al.*, *Phys. Rev. Lett.* **92**, 086801 (2004).
- [11] In this experiment, 14 MgPs showing vibronic transitions were investigated. Their photon images all exhibit ringlike patterns but some of them have one maximum missing or asymmetric shapes due to their environments.
- [12] H.-H. Tsai and M. C. Simpson, *J. Phys. Chem. A* **107**, 526 (2003).
- [13] J. A. Shelnutt *et al.*, *J. Am. Chem. Soc.* **113**, 4077 (1991).
- [14] S. W. Wu *et al.*, *Phys. Rev. Lett.* **93**, 236802 (2004).
- [15] A. Ghosh, *Acc. Chem. Res.* **31**, 189 (1998).
- [16] D. Spangler *et al.*, *J. Am. Chem. Soc.* **99**, 7478 (1977).
- [17] This broken degeneracy could be quantized by measuring the energy difference between the first peaks of type-I and type-II spectra. For various MgPs, these values vary from 13 to 40 meV at 765 nm (5 to 15 nm).
- [18] D. L. Mills, *Phys. Rev. B* **65**, 125419 (2002).
- [19] S. Wu and D. L. Mills, *Phys. Rev. B* **65**, 205420 (2002).
- [20] Details of the modeling and experimental results are described in a longer paper [C. Chen, P. Chu, C. A. Bobisch, D. L. Mills, and W. Ho (to be published)].
- [21] P. Chu and D. L. Mills, *Phys. Rev. B* **79**, 115435 (2009).
- [22] N. Lorente *et al.*, *Phys. Rev. Lett.* **86**, 2593 (2001).